Moiré trions in $MoSe_2/WSe_2$ heterobilayers

Xi Wang[1,2,#], Jiayi Zhu[1,#], Kyle L. Seyler[1], Pasqual Rivera[1], Huiyuan Zheng[3,4], Yingqi Wang[1], Minhao He[1], Takashi Taniguchi[5], Kenji Watanabe[6], Jiaqiang Yan[7,8], David G. Mandrus[7-9], Daniel R. Gamelin[2], Wang Yao[3,4,*], and Xiaodong Xu[1,10,*]

[1]Department of Physics, University of Washington, Seattle, WA, USA
[2]Department of Chemistry, University of Washington, Seattle, WA, USA
[3]Department of Physics, University of Hong Kong, Hong Kong, China
[4]HKU-UCAS Joint Institute of Theoretical and Computational Physics at Hong Kong, China
[5]International Center for Materials Nanoarchitectonics, National Institute for Materials Science, Tsukuba, Ibaraki 305-0044, Japan
[6]Research Center for Functional Materials, National Institute for Materials Science, Tsukuba, Ibaraki 305-0044, Japan
[7]Materials Science and Technology Division, Oak Ridge National Laboratory, Oak Ridge, Tennessee, 37831, USA
[8]Department of Materials Science and Engineering, University of Tennessee, Knoxville, Tennessee, 37996, USA
[9]Department of Physics and Astronomy, University of Tennessee, Knoxville, Tennessee, 37996, USA
[10]Department of Materials Science and Engineering, University of Washington, Seattle, WA, USA

Correspondence to: wangyao@hku.hk; xuxd@uw.edu

Abstract: Transition metal dichalcogenide moiré bilayers with spatially periodic potentials have emerged as a highly tunable platform for studying both electronic[1–6] and excitonic[4,7–13] phenomena. The power of such a system lies in the combination of strong Coulomb interactions with the capability of controlling the charge number in a moiré potential trap. Electronically, exotic charge orders at both integer and fractional fillings have been discovered[2,5]. However, the impact of charging effects on excitons trapped in moiré potentials is poorly understood. In this work, we report the observation of moiré trions and their doping dependent photoluminescence polarization in H-stacked $MoSe_2/WSe_2$ heterobilayers. We found that as moiré traps are filled with either electrons or holes, new sets of interlayer exciton photoluminescence peaks with narrow linewidths emerge about 7 meV lower in energy than the neutral moiré excitons. Circularly polarized photoluminescence reveals switching from co-circular to cross-circular polarizations as moiré excitons are changed from negatively charged and neutral to positively charged conditions. This switching results from the competition between valley-flip and spin-flip energy relaxation pathways of photo-excited electrons during interlayer trion formation. Our results offer a starting point for engineering both bosonic and fermionic many-body effects based on moiré excitons[14].

Main text

Heterostructures of monolayer semiconductors offer a powerful platform to explore light-matter interactions. Using $MoSe_2/WSe_2$ heterobilayers as an example, a type II band alignment leads to interlayer excitons with long population and polarization lifetimes[15]. With careful stacking to produce atomically clean heterostructure interfaces, a moiré superlattice can be formed with a periodically varying interlayer separation and electronic bandgap[16,17]. This periodic potential modulation of the electronic structure in real space functions as an ordered nanodot array and fundamentally modifies the interlayer exciton properties[8–12,18–21]. Quantum-dot-like moiré exciton photoluminescence (PL) with twist angle control of valley polarization and Landé g-factor have been reported[10,12,13]. Strong photon anti-bunching of moiré exciton has also been observed[13], implying its potential for quantum optoelectronic applications. In addition to hexagonal moiré superlattices, strain induced 1D moiré structures have been identified[9], which lead to linearly polarized moiré exciton luminescence, in contrast with the circularly polarized luminescence of the unstrained heterobilayers.

Besides moiré excitons, their charged counterparts, such as trions add a new dimension on controlling the interactions between excitons in the moiré traps (Fig. 1a). Unlike bosonic particles (excitons), the charge counterparts, trions, obeys fermionic statistics. Transport properties and responses to electric and magnetic field are significantly different between the two classes of particles. In addition to dipolar interaction, the trions can interact with each other through the long-range Coulomb interaction. The realization of charged moiré excitons is important for allowing an optically accessible platform to explore fermionic many-body effects. While rapid progress has been made in characterizing neutral moiré interlayer excitons, their charged counterparts however remain elusive. It is unclear whether moiré trions exist, and if so, how they compare to neutral ones.

In this work, we demonstrate formation of interlayer moiré trions in superlattices formed by stacked WSe_2 and $MoSe_2$ monolayers. Through electrostatic gating, we found that once the sample is electron- or hole-doped, new sets of moiré trion PL peaks appear ~7 meV lower in energy with respect to charge neutral moiré excitons. The Zeeman splitting of opposite polarized trion PL peaks is consistent with electron-hole valley pairing under H-type alignment. In addition, the spin optical polarization of the emitter is tuned with doping. When the system is hole doped, valley polarization of the positively charged moiré trion is inverted compared to both neutral and negatively charged ones. Such polarization inversion arises from the competition between spin-flip but valley conserved and spin-conserve but valley flipped relaxation channels of electrons in the formation of interlayer trions. The population lifetimes of moiré trions and excitons are also measured by time-resolved PL. Combining polarization-resolved excitation and detection, the valley polarization lifetime is found to be hundreds of nanoseconds.

The device structure with a dual-gated geometry is shown in Fig. 1b. The $WSe_2/MoSe_2$ heterobilayer is assembled by standard dry-transfer techniques with hexagonal boron nitride (BN) encapsulation and semi-transparent thin graphite top and bottom gates to independently control doping and vertical electric field effects. Edge contacts are used to connect both $MoSe_2$ and WSe_2 layers. All samples are H-stacked, i.e., with nearly 60^o twist angle. For the device presented in the main text, the moiré lattice constant is about 11nm, as determined by piezoresponse force microscopy[9,22] (Supplemental Figure S1). Multiple devices have been studied and show consistent results. All measurements are done with laser excitation at 1.713 eV (close to the WSe_2 A exciton resonance) at a temperature of 1.6 K, unless otherwise specified.

We first describe PL measurements of interlayer moiré excitons as a function of doping (Fig. 1c). Due to similar thicknesses of top and bottom BN, varying doping with a fixed zero displacement field is achieved by sweeping both gates together. The optical excitation power is 50 nW with the diameter of laser beam spot around 1 μm. The detection is unpolarized. Within the gate range corresponding to negligible doping (corroborated by gate-dependent reflectance measurements of the intralayer WSe_2 and $MoSe_2$ excitons[23] , Supplemental Figure S2), we observe several discrete PL lines near 1.396 eV, with linewidths as narrow as about 100 μeV. As reported previously[10,12,13], these emissions are from neutral interlayer excitons trapped in a moiré potential (M_X^0). The emission energy is nearly constant as doping varies, consistent with the fixed displacement field during gate sweep.

When the gate voltage becomes large enough to effectively inject electrons/holes to the heterobilayers, the M_X^0 PL intensity rapidly drops and a new set of peaks with narrow linewidths emerges lower energy. The doping dependence of these peaks resembles the oscillator strength transfer from neutral to charged excitons observed in monolayers[24,25]. Their narrow linewidths, similar to M_X^0 linewidths, suggest that they correspond to positively (M_T^+) and negatively (M_T^-) charged interlayer trions trapped in the moiré potential by hole and electron doping, respectively. Fig. 1d plots M_T^+ PL intensity as a function of temperature. The PL spectrum at 1.6K is overlaid on top. The PL intensity quickly fades above 10 K, consistent with the shallow moiré potential of about 30 meV in H-stacked $MoSe_2/WSe_2$ heterobilayers[21]. Note that the landscape of moiré potentials for electrons and holes are different. These facts can be responsible for the detailed exciton property difference between moiré traps, including PL intensity, energy, and exact gate range. For instance, this moiré potential inhomogeneity is likely responsible for the slight persistence of some neutral (trion) peaks into the hole doped (charge neutral) regime (see Supplemental Figure S3 for additional data taken at different spots).

In $MoSe_2/WSe_2$ heterobilayers, the lowest energy conduction band is in the $MoSe_2$ layer and the highest energy valance band is in the WSe_2 layer[26]. The band offsets are several hundred meV. Therefore, the energetically favorable configuration for moiré trions consists of two electrons (holes) in the same layer and one hole (electron) in the opposite layer[27], as depicted in the insets of Fig. 1c. For example, M_T^+ has the two holes in WSe_2 layer and the electron in $MoSe_2$ layer. Due to inhomogeneous moiré effects, we cannot assign the exact one to one correspondence between trions and neutral ones. To obtain trion binding energy, we extract the energy difference between the center of the group of peaks (white frames in Supplemental Figure S4), which is about 7 meV. This peak difference is consistent across the different spots in the same sample and confirmed by the second sample (Supplemental Figure S5). Free interlayer trions with about 10 meV photoluminescence linewidth have been reported in MoSe2/WSe2 heterobilayer[28], where positively and negatively charged ones have binding energy of 10 and 15 meV, respectively. The weaker binding energy of moiré trapped trion is intuitively expected, as the confinement from the moiré potential has limited the variation of wavefunction to reach the maximum binding. The exact quantification of the trion binding energy in moiré potential is a nontrivial task due to the close length scales of moiré confinement and Bohr radius, as well as the comparable energy scales of the quantization in the moiré potential and the trion binding energy. Future theory work is needed to address this interesting problem.

Interlayer excitons have permanent out-of-plane electric dipoles, which enable tuning of their energy via a DC stark effect[29]. Though trapped with moiré potential, the moiré trions energy also adopt DC stark effect (30 meV over 0.1V/nm change of electric field). Applying an out-of-plane

displacement field, all three emissive species (M_T^-, M_T^+, M_X^0) show similar linear energy shifts in PL spectra. As an example, Fig. 1e shows the PL peak positions of M_T^- as a function of out-of-plane electric field. The energy shift is about $\Delta \sim 30$ meV by a change of electric field of $E \sim 0.1$V/nm. We estimate Δ/E as 0.2927 ± 0.0001 $e{\cdot}nm$ for M_T^-, 0.2874 ± 0.0015 $e{\cdot}nm$ for M_T^+, and 0.2906 ± 0.0007 $e{\cdot}nm$ for M_X^0 (Supplemental Figure S6). From simple electrostatics, Δ/E in TMDs is approximately $\frac{\varepsilon_{BN}}{\varepsilon_{TMD}} ed$. Using $\varepsilon_{BN} \sim 3$ and $\varepsilon_{TMD} \sim 7$ for the out-of-plane dielectric constants of BN and TMDs[4,30], respectively, we estimate an effective interlayer separation d of about 0.68 nm.

As demonstrated previously[10,12,13], Landé g factors are a fingerprint to distinguish excitons trapped in moiré potentials from those bound to atomic defects. The g factor of a bright interlayer exciton is determined by the valley index (τ_c, τ_v) of its constituent electron and hole. Here, valley index $\tau = \pm 1$ corresponds to $\pm K$ valleys. Due to the smooth trapping potential of a moiré superlattice, moiré excitons inherit the g-factors of free interlayer excitons. For H-stacked $MoSe_2/WSe_2$ heterobilayers, the g factor of M_X^0 in the triplet configuration has been identified as about -16[10,31]. Figure 2 plots PL intensities as a function of perpendicular magnetic field for three fixed doping levels corresponding to M_T^- (Fig. 2a), M_X^0 (Fig. 2b), and M_T^+ (Fig. 2c). Due to valley Zeeman splitting, the peak energies with σ^- (E_{σ^-}) and σ^+ (E_{σ^+}) polarized PL differ in the presence of the magnetic field. Each moiré exciton species exhibits the X pattern in the intensity plot. Although inhomogeneity of moiré traps gives rise to a distribution of neutral and charged moiré exciton peak energies, the peak energy shifts as a function of magnetic field are nearly the same for all moiré emitters. This behavior is characteristic of excitons trapped in a moiré potential[10].

We can define the Zeeman splitting between the PL peaks as $\Delta E = E_{\sigma^+} - E_{\sigma^-}$, which is to be distinguished from the valley Zeeman splitting. The latter has a value determined by the valley pairing (R vs. H stacking) and spin pairing (singlet vs. triplet) only, while ΔE above can be different from the valley Zeeman splitting by a sign determined by the valley optical selection rule[10], i.e., negative (positive) if K valley emits σ^+ (σ^-) polarized light. The extracted ΔE values for M_T^-, M_X^0, and M_T^+ are shown in Fig. 2d, 2e, and 2f. Linear fits of ΔE yield a g factor of -16.08 $\pm$ 0.01 for M_X^0, and effective g factors (g') of -16.07 $\pm$ 0.01 and –16.44 $\pm$ 0.07 for M_T^- and M_T^+, respectively. Neglecting the possible contribution to the Zeeman splitting by the carrier interaction effects, the effect of magnetic field on trion energy can be seen as the sum of the Zeeman shift of a valley exciton and that of the extra carrier. Thus, the extra electron/hole in a trion only shifts the transition energy but does not contribute to the spectroscopic Zeeman splitting ΔE, defined as the PL peak energy differences in the magnetic field. The similarity of these g and g' values (about -16) supports our assumption and the assignment of all of these narrow lines as excitons/trions trapped in the smooth moiré potential traps. It also implies that the electron-hole pairs involved in the radiative recombination all have the spin-triplet configuration.

A unique feature of the moiré trap is the three-fold rotation symmetry of local atomic registry, which results in circularly polarized valley optical selection rules[21]. To investigate moiré trion valley polarization, we performed helicity resolved PL measurements as a function of doping. Figures 3a and b are the PL intensity plots with σ^+ (Fig. 3a) and σ^- (Fig. 3b) polarized detection under σ^+-polarized optical pumping. Fig. 3c shows the corresponding valley polarization. Here, we define valley polarization as $\rho = \frac{I_{\sigma+} - I_{\sigma-}}{I_{\sigma+} + I_{\sigma-}}$, where $I_{\sigma^\pm}$ is the $\sigma^\pm$ polarized PL intensity. The polarization resolved spectra collected at selected doping levels are also shown in Fig. 3d. As

demonstrated[10], M_X^0 is strongly co-circularly polarized. Upon doping with excess carriers, the optical polarization of the moiré trions is tunable. Both M_T^- and M_T^+ have appreciable circular polarization in their PL, but opposite sign (see also an additional device D2 with data in Supplemental Fig. S5). As shown in Fig. 3c, M_T^- is co-circularly polarized with the pump, like M_X^0, with degree of polarization as high as 90%. Whereas M_T^+ is changed to cross-circularly polarized PL with much smaller ρ.

There are a few possible explanations for the gate-tunable PL polarization. For instance, gating can switch the lowest energy moiré sites with opposite valley optical selection rules in a supercell[21]. Experimental signature of this effect has been recently reported[32]. This optical selection rule switching should lead to opposite sign of the polarization Zeeman splitting between M_T^- and M_T^+. However, this is not the case here. Instead, such a polarization reversal behavior is more appropriately explained by the competition between spin conserved valley-flip channel and valley conserved spin-flip relaxation channels of electrons during the interlayer trion formation process. For all three charge configurations, the recombining electron-hole pair is trapped at the same moiré site. Without altering the optical selection rule, the measured polarization Zeeman splitting (or g factor) would not change appreciably both in sign and magnitude, consistent with our experimental observation (Fig. 2). Below we illustrate the physical picture under σ^+ polarized excitation with details given in supplementary material Section S1 and Figure S7.

In both electron-doped and charge-neutral cases, the spin-valley index of the photo-excited hole determines the emission polarization of the M_T^- or M_X^0. For simplicity, the valley notation of WSe_2 and $MoSe_2$ are assigned as $\pm K$ and $\pm K'$, respectively. In the H stacking configuration (i.e., $MoSe_2$ is nearly 60 degree rotated with respect to WSe_2), K $(-K)$ and $-K'$ (K') are nearly aligned in the momentum space. When the σ^+ excitation is at the WSe_2 monolayer exciton resonance, the photo-created holes are predominantly at the K valley band edge, with the polarization protected by the spin-valley locking. The K valley hole in WSe_2 is momentum aligned with the $-K'$ valley electron in $MoSe_2$ band edge to form a recombining pair in spin triplet configuration (Fig. 3e, top and middle panels). From the observed co-circular PL polarization with the pump, we can further determine that these moiré excitons/trions are trapped at the H_h^h local of the moiré supercell[33]. The high helicity indicates the valley polarization is well-protected by spin-valley locking. The slight difference in polarization between M_X^0 and M_T^- can arise from the difference of electron population distribution between the valleys as the former is from photoexcited electrons while the latter has contribution from electrostatic doping.

We have also examined the excitation frequency dependence of the PL polarization. Upon excitation at the $MoSe_2$ monolayer exciton resonance, the σ^+ excitation creates holes in the $MoSe_2$ K' valley, which relaxes to the WSe_2 band edge, ending up either in $-K$ valley through the spin-flip interlayer hopping, or K valley through the valley-flip hopping. The competition of these two relaxation channels determines the hole valley polarization at the WSe_2 band edge, resulting in a reduced (M_T^-) or even vanishing emission polarization (M_X^0). These understanding are consistent with our polarization-dependent photoluminescence excitation spectroscopy, as shown in supplementary Figure S8.

For the hole doped case, the M_T^+ consists of two holes at opposite valleys. Thus, its electron valley configuration determines the emission polarization (Fig. 3e, bottom panel). Unlike the hole, photo-created electron needs to go to the $MoSe_2$ band edge by interlayer hopping and energy relaxation, which also requires either a spin-flip or a valley-flip in H-stacked $MoSe_2/WSe_2$. Spin-

flip and valley-flip of the electron in the relaxation process can be facilitated respectively by the Γ_5 phonon at zone center, and K_3 phonon at zone edge[34]. Previous work[34] has found that the valley flip rate exceeds the spin-flip one. These relaxation channels can place the photo-created electrons at either valley of the $MoSe_2$ band edge (see supplementary materials Fig. S7). Their competition leads to a smaller polarization with a reversed helicity of the M_T^+ PL compared to that of both M_T^- and M_X^0.

Lastly, we examine the valley relaxation dynamics of both neutral and charged moiré excitons by time and polarization resolved PL at selected gate voltages. Figure 4 presents the decay of co-polarized (red) and cross-polarized (blue) PL of M_T^- (Fig. 4a) and M_X^0 (Fig. 4b) of Device 2. The polarization of M_T^+ is a bit small for a reliable measurement. The excitation power is 100 nW. The corresponding valley polarization dynamics are shown in Figs. 4c-d. Single exponential fits (solid lines) to valley polarization decay yields lifetimes of about 370 ns and 1 μs for M_T^- and M_X^0, respectively. These lifetimes are much longer than those of monolayer excitons and trions, indicating the possibilities for engineering both bosonic and fermionic many-body effects with dynamic control based on moiré emitter arrays.

Methods

Sample fabrication. Mechanically exfoliated monolayers of $MoSe_2$ and WSe_2 are stacked using a dry-transfer technique. The crystal orientation of the individual monolayers was first determined by linear-polarization resolved second-harmonic generation before transfer. The alignment angle of $MoSe_2$ and WSe_2 is double checked by piezoresponse force microscopy during transfer before encapsulating with bottom hexagonal boron nitride (BN). The BN encapsulation (10–30 nm) provides an atomically smooth substrate.

Photoluminescence measurements. PL measurements are performed in a home-built confocal microscope in reflection geometry. The sample is mounted in an exchange-gas cooled cryostat equipped with a 9 T superconducting magnet in Faraday configuration. The sample temperature is kept at 1.6 K unless otherwise specified. A power-stabilized and frequency-tunable narrow-band continuous-wave Ti:sapphire laser (M2 SolsTiS) is used to excite the sample unless otherwise specified. The photoluminescence is spectrally filtered from the laser using a long-pass filter before being directed into a spectrometer. The PL signals are dispersed by a diffraction grating (1,200 grooves per mm) and detected on a silicon CCD camera. Polarization-resolved PL is obtained based on a combination of quarter-wave plates, half-wave plates, and linear polarizers for excitation and collection. Time-resolved PL data are acquired using a time-correlated single-photon counting module (PicoHarp 300) with a supercontinuum fiber laser (pulse duration around 10 ps; repetition rate around 3 MHz; average power 100 nW) at 720 nm for excitation and a silicon avalanche photodiode for detection. The narrow emission lines were spectrally filtered (collection width of about 2 meV) through a spectrometer before detection on the avalanche photodiode.

Calibration of doping density and electric field. The doping densities in the heterobilayer are determined from the applied gate voltages based on a parallel-plate capacitor model[23]. The thickness of BN is determined by atomic force microscopy. Both top and bottom BN flakes of the device presented in maintext are 20 nm. The doping density is calculated as $C_b\Delta V_b + C_t\Delta V_t$, where C_t and C_b are the capacitance of top and bottom gates. ΔV_t and ΔV_b are the applied gate voltages relative to the level of the valence/conduction band edge. The geometric capacitance $C_t = C_b$ is about 133 nF with dielectric constant $\varepsilon_{hBN} \sim 3$ (Ref [35]). The out of plane electric displacement field is calculated as $D = (V_b C_b - V_t C_t)/2\varepsilon_0$ and electric field $E = D/\varepsilon_{BN}$.

Acknowledgments: Research on moiré trions is primarily supported as part of Programmable Quantum Materials, an Energy Frontier Research Center funded by the U.S. Department of Energy (DOE), Office of Science, Basic Energy Sciences (BES), under award DE-SC0019443. Zeeman-splitting and time-resolved measurements are mainly supported by DoE BES under award DE-SC0018171. Device fabrication is partially supported by Army Research Office (ARO) Multidisciplinary University Research Initiative (MURI) program (grant no. W911NF-18-1-0431) and NSF EFRI (Grant No. 1741656). The AFM-related measurements were performed using instrumentation supported by the U.S. National Science Foundation through the UW Molecular Engineering Materials Center (MEM·C), a Materials Research Science and Engineering Center (DMR-1719797). WY and HZ acknowledge support by the Croucher Foundation (Croucher Senior Research Fellowship) and the Research Grants Council of Hong Kong (17302617). DM and JY are supported by the US Department of Energy, Office of Science, Basic Energy Sciences, Materials Sciences and Engineering Division. KW and TT acknowledge the support from the Elemental Strategy Initiative conducted by the MEXT, Japan, Grant Number JPMXP0112101001, JSPS KAKENHI Grant Numbers JP20H00354 and the CREST(JPMJCR15F3), JST. XX acknowledges the support from the State of Washington funded Clean Energy Institute and from the Boeing Distinguished Professorship in Physics.

Author contributions:
X.X. and W.Y. conceived the experiment. X.W. and J.Z. fabricated the samples, assisted by Y.W. and M.H.. X.W. and J.Z. performed the measurements. K.S. and P.R. fabricated and measured Device D2. X.W., J.Z., H.Z. X.X., W.Y., and D.G. analyzed and interpreted the results. T.T. and K.W. synthesized the BN crystals. J.Y. and D.M. synthesized and characterized the bulk WSe_2 and $MoSe_2$ crystals. X.W., X.X., W.Y., and D.G. wrote the paper with input from all authors. All authors discussed the results.

Competing Interests: The authors declare no competing financial interests.

Data Availability: The datasets generated during and/or analyzed during this study are available from the corresponding author upon reasonable request.

References:

1. Shimazaki, Y. *et al.* Strongly correlated electrons and hybrid excitons in a moiré heterostructure. *Nature* **580**, 472–477 (2020).
2. Regan, E. C. *et al.* Mott and generalized Wigner crystal states in WSe2/WS2 moiré superlattices. *Nature* **579**, 359–363 (2020).
3. Tang, Y. *et al.* Simulation of Hubbard model physics in WSe2/WS2 moiré superlattices. *Nature* **579**, 353–358 (2020).
4. Sung, J. *et al.* Broken mirror symmetry in excitonic response of reconstructed domains in twisted MoSe2/MoSe2 bilayers. *Nat. Nanotechnol.* **15**, 750–754 (2020).
5. Xu, Y. *et al.* Correlated insulating states at fractional fillings of moiré superlattices. *Nature* **587**, 214–218 (2020).
6. Wang, L. *et al.* Correlated electronic phases in twisted bilayer transition metal dichalcogenides. *Nat. Mater.* **19**, 861–866 (2020).
7. Jin, C. *et al.* Observation of moiré excitons in WSe2/WS2 heterostructure superlattices.

Nature **567**, 76–80 (2019).
8. Alexeev, E. M. *et al.* Resonantly hybridized excitons in moiré superlattices in van der Waals heterostructures. *Nature* **567**, 81–86 (2019).
9. Bai, Y. *et al.* Excitons in strain-induced one-dimensional moiré potentials at transition metal dichalcogenide heterojunctions. *Nat. Mater.* **19**, 1068–1073 (2020).
10. Seyler, K. L. *et al.* Signatures of moiré-trapped valley excitons in MoSe2/WSe2 heterobilayers. *Nature* **567**, 66–70 (2019).
11. Tran, K. *et al.* Evidence for moiré excitons in van der Waals heterostructures. *Nature* **567**, 71–75 (2019).
12. Brotons-Gisbert, M. *et al.* Spin–layer locking of interlayer excitons trapped in moiré potentials. *Nat. Mater.* **19**, 630–636 (2020).
13. Baek, H. *et al.* Highly energy-tunable quantum light from moiré-trapped excitons. *Sci. Adv.* **6**, 1–7 (2020).
14. Combescot, M., Betbeder-Matibet, O. & Dubin, F. The many-body physics of composite bosons. *Phys. Rep.* **463**, 215–320 (2008).
15. Rivera, P. *et al.* Interlayer valley excitons in heterobilayers of transition metal dichalcogenides. *Nat. Nanotechnol.* **13**, 1004–1015 (2018).
16. Zhang, C. *et al.* Interlayer couplings, Moiré patterns, and 2D electronic superlattices in MoS2/WSe2 hetero-bilayers. *Sci. Adv.* **3**, 1–8 (2017).
17. Wilson, N. R. *et al.* Determination of band offsets, hybridization, and exciton binding in 2D semiconductor heterostructures. *Sci. Adv.* **3**, 1–8 (2017).
18. Ruiz-Tijerina, D. A. & Fal'Ko, V. I. Interlayer hybridization and moiré superlattice minibands for electrons and excitons in heterobilayers of transition-metal dichalcogenides. *Phys. Rev. B* **99**, 30–32 (2019).
19. Yuan, L. *et al.* Twist-angle-dependent interlayer exciton diffusion in WS2–WSe2 heterobilayers. *Nat. Mater.* **19**, 617–623 (2020).
20. Li, W., Lu, X., Dubey, S., Devenica, L. & Srivastava, A. Dipolar interactions between localized interlayer excitons in van der Waals heterostructures. *Nat. Mater.* **19**, 624–629 (2020).
21. Yu, H., Liu, G. Bin, Tang, J., Xu, X. & Yao, W. Moiré excitons: From programmable quantum emitter arrays to spin-orbit–coupled artificial lattices. *Sci. Adv.* **3**, 1–8 (2017).
22. McGilly, L. J. *et al.* Visualization of moiré superlattices. *Nat. Nanotechnol.* **15**, 580–584 (2020).
23. Wang, Z., Zhao, L., Mak, K. F. & Shan, J. Probing the Spin-Polarized Electronic Band Structure in Monolayer Transition Metal Dichalcogenides by Optical Spectroscopy. *Nano Lett.* **17**, 740–746 (2017).
24. Mak, K. F. *et al.* Tightly bound trions in monolayer MoS 2. *Nat. Mater.* **12**, 207–211 (2013).
25. Ross, J. S. *et al.* Electrical control of neutral and charged excitons in a monolayer semiconductor. *Nat. Commun.* **4**, 1–6 (2013).
26. Ross, J. S. *et al.* Interlayer Exciton Optoelectronics in a 2D Heterostructure p-n Junction. *Nano Lett.* **17**, 638–643 (2017).
27. Bondarev, I. V. & Vladimirova, M. R. Complexes of dipolar excitons in layered quasi-two-dimensional nanostructures. *Phys. Rev. B* **97**, 1–11 (2018).
28. Jauregui, L. A. *et al.* Electrical control of interlayer exciton dynamics in atomically thin heterostructures. *Science (80-.).* **366**, 870–875 (2019).

29. Rivera, P. *et al.* Observation of long-lived interlayer excitons in monolayer MoSe 2-WSe 2 heterostructures. *Nat. Commun.* **6**, 4–9 (2015).
30. Tang, Y. *et al.* Tuning layer-hybridized moiré excitons by the quantum-confined Stark effect. *Nat. Nanotechnol.* **2**, (2020).
31. Wang, T. *et al.* Giant Valley-Zeeman Splitting from Spin-Singlet and Spin-Triplet Interlayer Excitons in WSe2/MoSe2 Heterostructure. *Nano Lett.* **20**, 694–700 (2020).
32. Ciarrocchi, A. *et al.* Polarization switching and electrical control of interlayer excitons in two-dimensional van der Waals heterostructures. *Nat. Photonics* **13**, 131–136 (2019).
33. Yu, H., Liu, G. Bin & Yao, W. Brightened spin-triplet interlayer excitons and optical selection rules in van der Waals heterobilayers. *2D Mater.* **5**, 035021 (2018).
34. He, M. *et al.* Valley phonons and exciton complexes in a monolayer semiconductor. *Nat. Commun.* **11**, 1–7 (2020).
35. Movva, H. C. P. *et al.* Density-dependent quantum hall states and Zeeman splitting in monolayer and Bilayer WSe2. *arXiv* **1**, 1–5 (2017).

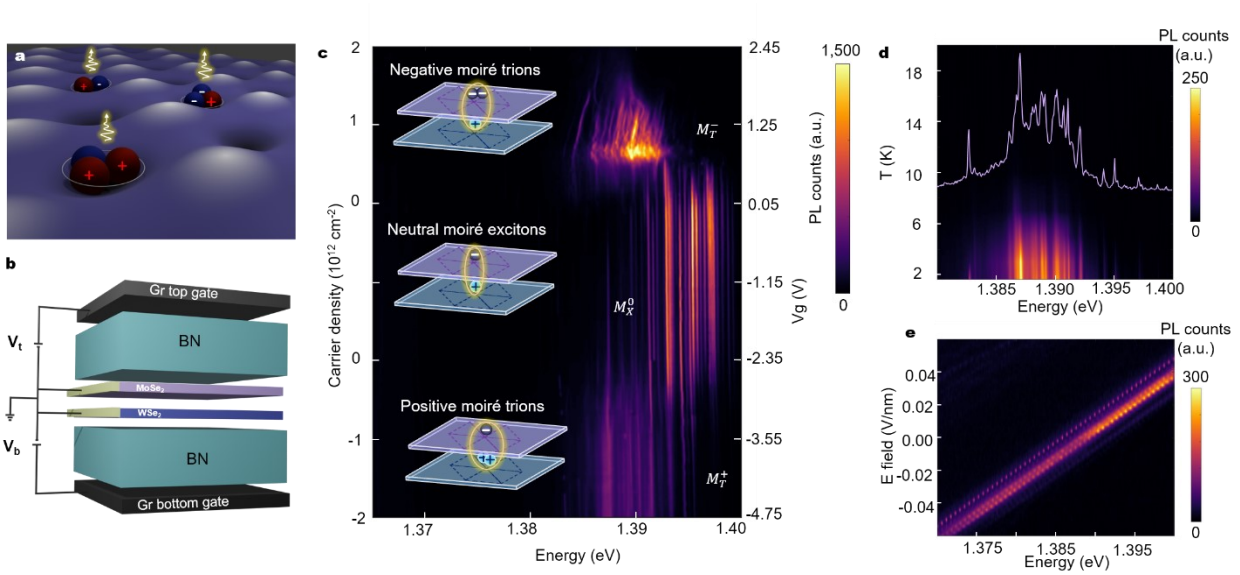

Figure 1 | Moiré trions are formed with electrostatic gating. a, Schematics of neutral and charged excitons in moiré traps. **b**, Schematics of double-BN encapsulated devices with dual graphite gates. **c**, Photoluminescence (PL) intensity plot as a function of doping and photon energy. At both electron and hole doping, new sets of peaks form at ~7 meV lower energy, with a rapid drop in the PL intensity of the charge neutral moiré exciton. Insets depict the charge configuration of both neutral and charged excitons. **d**, Temperature dependent PL intensity plot at a fixed hole doping, showing the shallow potential of moiré traps. Inset is the PL spectrum collected at 1.6 K. **e**, PL spectra of negative moiré trions versus electric field applied out of plane with fixed doping.

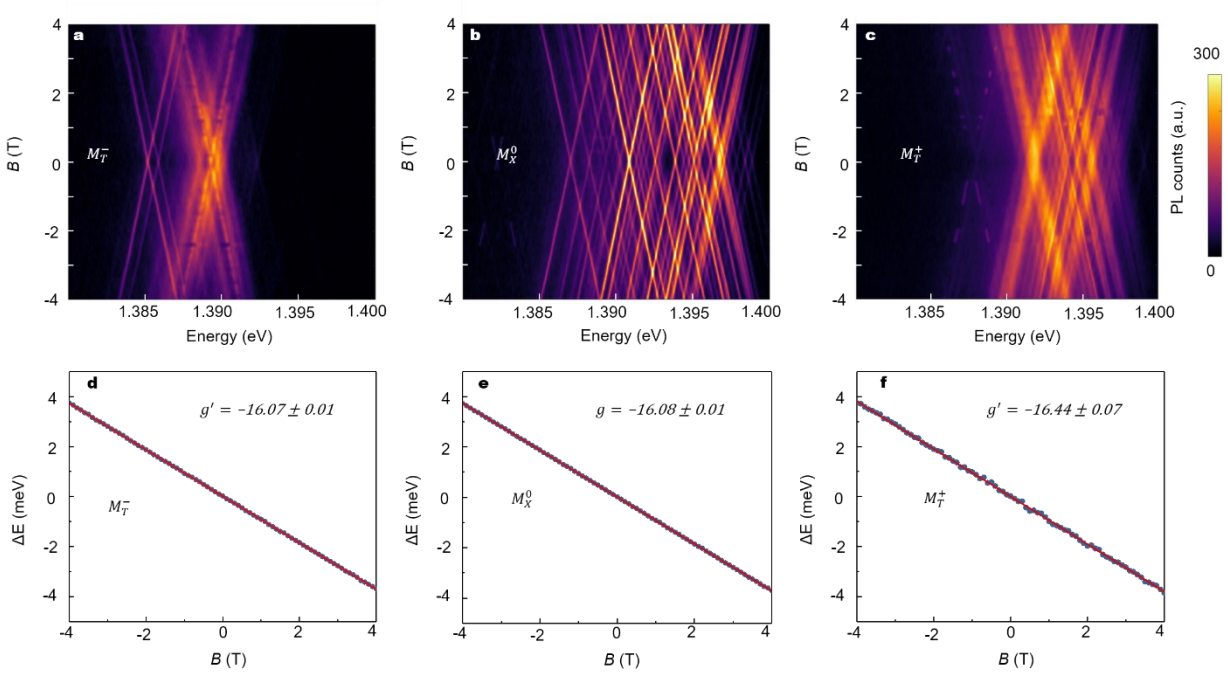

Figure 2 | Zeeman splitting of both neutral and charged moiré excitons. The obtained effective *g* factors are consistent with moiré traps in H-type alignment. **a-c**, Magneto-PL of negative charged, neutral, and positive charged moiré excitons. The excitation is linearly polarized with both right-circularly and left-circularly polarized emission detection. **d-f**, Energy differences between right- and left-circularly polarized PL as a function of magnetic field extracted from panels (a-c). The corresponding effective g factors are calculated based on linear fits, as shown in the figures.

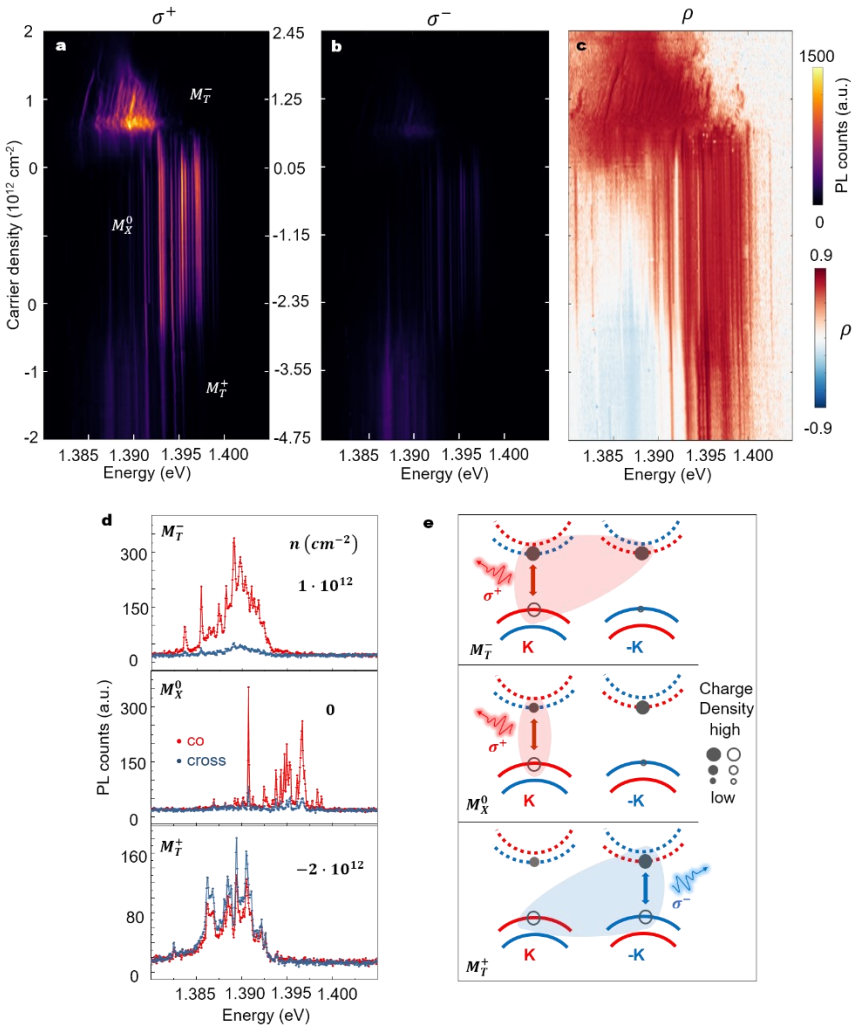

Figure 3 | Doping dependent valley polarization of moiré trions. a-b, Helicity resolved PL intensity plots as a function of doping. The σ^+ and σ^- polarized components are shown in **a** and **b**, respectively, with σ^+ polarized excitation. **c**, Degree of PL polarization (ρ) as a function of doping, calculated from **a**-**b**. **d**, Helicity resolved PL spectra at selected doping n, for negatively charged M_T^- (top), neutral M_X^0 (middle), and positively charged M_T^+ (bottom) moiré excitons. The PL from M_T^- and M_X^0 are co-circularly polarized, whereas PL from M_T^+ is cross-circularly polarized. **e**, Schematics illustrating doping dependent PL polarization of the moiré exciton/trions. The conduction (dashed lines) and valence (solid lines) are from $MoSe_2$ and WSe_2, respectively. Electron and hole are represented by solid and open circles. Red and blue indicate the spin orientations. The density of charge carriers (electrons/holes) are indicated by the size of circles (solid/open) shown in the inset. The valley index of the majority hole (electron) population determines the PL helicity of M_T^- and M_X^0 (M_T^+).

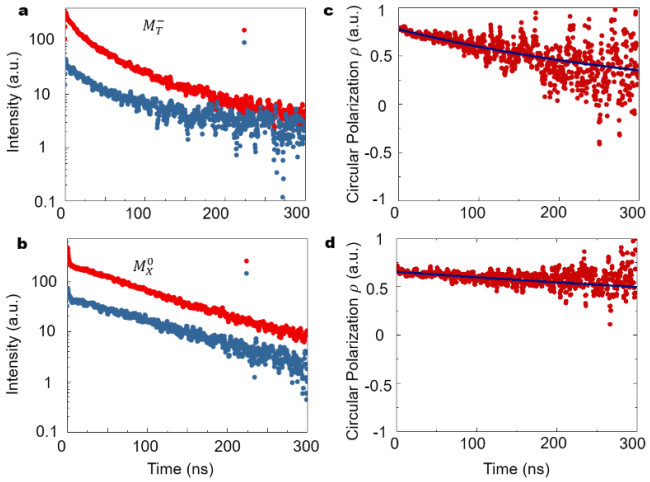

Figure 4 | Moiré exciton and trions dynamics. a-b, Time- and helicity-resolved PL of **a**, M_T^-, and **b**, M_X^0. The corresponding valley polarization dynamics are shown in **c** & **d**. Solid lines are exponential fits to valley polarization decay, with lifetimes of around 370 ns and 1 μs for M_T^- and M_X^0, respectively.